Published in final edited form as:
Neurobiol Aging. 2013 March ; 34(3): 832–844. doi:10.1016/j.neurobiolaging.2012.07.010.

CREB-binding protein (CBP) levels in the rat hippocampus fail to predict chronological or cognitive aging

Inês Tomás Pereira[a,b], **Christopher E. Coletta**[c], **Evelyn V. Perez**[b], **David H. Kim**[b], **Michela Gallagher**[d], **Ilya G. Goldberg**[c], and **Peter R. Rapp**[b]

[a]Neuroscience Graduate Program, Mount Sinai School of Medicine, One Gustave L. Levy Place, New York, NY 10029, United States

[b]Neurocognitive Aging Section, Laboratory of Experimental Gerontology, National Institute on Aging, NIH, 251 Bayview Blvd, Baltimore, MD 21224, United States

[c]Image Informatics and Computational Biology Unit, Laboratory of Genetics, National Institute on Aging, NIH, 251 Bayview Blvd, Baltimore, MD 21224, United States

[d]Department of Psychological and Brain Sciences, Johns Hopkins University, 3400 N Charles St, Ames Hall, Baltimore, MD 21218, United States

Abstract

Normal cognitive aging is associated with deficits in memory processes dependent on the hippocampus, along with large-scale changes in the hippocampal expression of many genes. Histone acetylation can broadly influence gene expression and has been recently linked to learning and memory. We hypothesized that cAMP response element binding (CREB)-binding protein (CBP), a key histone acetyltransferase, may contribute to memory decline in normal aging. Here, we quantified CBP protein levels in the hippocampus of young, aged unimpaired and aged impaired rats, classified on the basis of spatial memory capacity documented in the Morris water maze. First, CBP-immunofluorescence was quantified across the principal cell layers of the hippocampus using both low and high resolution laser scanning imaging approaches. Second, digital images of CBP immunostaining were analyzed by a multi-purpose classifier algorithm (WND-CHARM) with validated sensitivity across many types of input materials. Finally, CBP protein levels in the principal subfields of the hippocampus were quantified by quantitative western blotting. CBP levels were equivalent as a function of age and cognitive status in all analyses. The sensitivity of the techniques used was substantial, sufficient to reveal differences across the principal cell fields of the hippocampus, and to correctly classify images from young and aged animals independent of CBP-immunoreactivity. The results are discussed in the context of recent evidence suggesting that CBP decreases may be most relevant in conditions of aging that, unlike normal cognitive aging, involve significant neuron loss.

Correspondence: Peter R. Rapp, Laboratory of Experimental Gerontology, National Institue on Aging, 251 Bayview Blvd, Suite 100, Baltimore, MD 21224, Phone: 410-558-8195, Fax: 410-558-8302, rappp@mail.nih.gov.

Disclosure Statement

The authors declare no conflicts of interest. All procedures were approved by the Johns Hopkins University and NIA Intramural Research Program Institutional Animal Care and Use Committees, in accordance with the National Institutes of Health Guide for the Care and Use of Laboratory Animals.

Keywords

epigenetics; memory; image analysis; stereology; quantitative microscopy

1. Introduction

Epigenetic regulation of gene transcription has recently been linked to learning and memory in several behavioral settings. In the hippocampus, histone acetylation increases as a consequence of both fear conditioning (Levenson, et al., 2004) and training in the Morris water maze (Bousiges, et al., 2010). Pharmacological inhibition of histone deacetylase (HDAC) enhances histone acetylation with an associated effect on behavior, improving long-term memory for object recognition (Stefanko, et al., 2009) and reversing the fear conditioning deficits seen in a mouse model of Alzheimer's disease (Kilgore, et al., 2010). In parallel with these results, levels of cAMP response element binding (CREB)-binding protein (CBP) and histone acetyltransferase (HAT) activity are increased following Morris water maze training in rats (Bousiges, et al., 2010).

CBP is a transcriptional co-activator with innate HAT activity. Mutations of the CBP gene in humans cause Rubinstein-Taybi Syndrome, which among other symptoms, includes severe mental retardation (Petrij, et al., 1995). Several mutant mouse models targeting CBP have been generated (Alarcón, et al., 2004, Bourtchouladze, et al., 2003, Chen, et al., 2010, Korzus, et al., 2004, Oike, et al., 1999, Valor, et al., 2011, Wood, et al., 2006), and although effects differ somewhat across models, robust impairment in memory mediated by the hippocampus is observed in each case. In one study, for example, memory assessed by both an object recognition task and the Morris water maze was significantly impaired in mice expressing an inducible dominant-negative CBP transgene that specifically blocked HAT activity while sparing CBP transcriptional coactivator function (Korzus, et al., 2004). Object recognition deficits observed in this model were rescued by pharmacological treatment with the HDAC inhibitor Trichostatin A, confirming the critical role of HAT activity.

Impairment in hippocampal learning and memory, and associated deficits in neuronal plasticity, are common features of aging across rodents, nonhuman primates, and humans (for review, see Fletcher and Rapp, 2012, Rosenzweig and Barnes, 2003). Whereas substantial neuron death and gross structural alteration do not appear to provide a basis for age-related cognitive decline in the absence of disease (Rapp and Gallagher, 1996, Rasmussen, et al., 1996), current evidence points to a substantially altered pattern of gene expression relevant to plasticity (Nyffeler, et al., 2007, Penner, et al., 2010, Smith, et al., 2000, VanGuilder, et al., 2010). In a recent study using the same well-characterized rat model of cognitive aging as the current investigation, for example, microarray analysis revealed that individual differences in the status of spatial learning and memory among aged subjects are coupled with changes in a broad array of genes involving multiple pathways, particularly in the CA3 field of the hippocampus (Haberman, et al., 2009). Prompted by these findings and related data from other microarray experiments (e.g. Rowe, et al., 2007), we reasoned that changes in chromatin regulation might be among the mechanisms that contribute to altered patterns of gene expression in the aged hippocampus. Although a previous study had reported substantial reductions in CBP immunoreactivity in the aged rat neocortex and hippocampus, relative to young adults (Chung, et al., 2002), potential links with the cognitive outcome of aging were not examined. A comprehensive assessment might also benefit from a combination of methodological approaches, aimed at confirming the effects of aging on both the magnitude and cellular distribution of changes in CBP. Accordingly, here we applied a battery of independent digital imaging, biochemical, and image classification tools to test the specific proposal that changes in baseline hippocampal

CBP levels contribute to variability in the effects of aging on spatial learning and memory. Contrary to expectations, the findings provide compelling evidence that CBP content can remain stable in the aged hippocampus, and that robust age-related deficits in hippocampal memory can occur in the absence of alterations in levels of this important HAT.

2. Methods

2.1 Subjects

Male Long-Evans rats (Charles River Laboratories, Raleigh, NC, USA) were housed individually in a vivarium at Johns Hopkins University, and maintained on a 12 hr light/dark cycle with food and water available *ad libitum*. Animals were examined for health and maintained under specific pathogen-free conditions throughout the study. Young adults (Y; n = 17) were 6 months and aged rats (n = 34) were 24 to 28 months old at time of sacrifice. All procedures were approved by the Johns Hopkins University and NIA Intramural Research Program Institutional Animal Care and Use Committees, in accordance with the National Institutes of Health Guide for the Care and Use of Laboratory Animals.

2.2 Standard water maze characterization

The water maze consisted of a circular tank (1.83 m in diameter), filled with tepid water (~25°C) made opaque with non-toxic white tempera paint. The hidden escape platform was located 1 cm below the water surface and maintained in a constant location across training trials. White curtains with conspicuous visual cues surrounded the maze to facilitate spatial navigation. Spatial learning and memory capacity was assessed according to the protocol described in Gallagher, et al. (1993). Training was conducted over eight consecutive days, three trials per day, with inter-trial intervals of 60 s. The location of the hidden platform remained constant, but the starting location varied among four equidistant points around the perimeter of the water maze. Every sixth trial was a probe test during which the platform was retracted and unavailable for 30 s, after which it was raised to allow animals to escape. A learning index score, validated in many earlier studies (Gallagher, et al., 2003, Haberman, et al., 2009, Smith, et al., 2000) was calculated as a weighted average of an animal's proximity to the platform location across probe trials (Gallagher, et al., 1993). By this measure, lower scores denote decreased search error reflecting the animal's focus on the acquired escape location. Earlier probe trials influence the learning index more heavily than later probe trials such that rapid acquisition yields relatively better (lower) scores. Based on data from a large number of animals, aged rats with learning index scores exceeding normative adult values were classified as aged-impaired (AI), and those that scored within the range of the Y group were designated aged-unimpaired (AU).

Since sensorimotor and motivational factors can impact performance in the spatial variant of the task, the day after completion of the 8-day learning protocol, animals were tested on a cued version. This procedure consisted of a single session of six trials in which a raised platform was visible above the water surface and varied pseudo-randomly in location across trials. Animals impaired in the cued version of the task were excluded from further analysis.

2.3 Immunohistochemistry

2.3.1 Tissue collection—Animals used for immunohistochemical analysis (11Y, 9AU and 11AI) were sacrificed directly from the home cage not less than two weeks following the conclusion of water mazing testing, with the testing to sacrifice interval held constant across groups, providing a window on baseline constitutive levels of CBP. Subjects were deeply anesthetized with 5% isoflurane and perfused transcardially at a rate of 35 ml/min with cold phosphate-buffered saline (PBS) for 2 min followed by ice-cold 4% paraformaldehyde in PBS (pH 7.2–7.4) for 13 min. After perfusion, brains were removed

and post-fixed in 4% paraformaldehyde in PBS for approximately 24 hr. The tissue was cryoprotected successively overnight in 10% followed by 20% glycerol at 4°C. Brains were then frozen in 2-methylbutane and stored at −80°C until sectioning in the coronal plane on a freezing sliding microtome at a nominal thickness of 50 μm.

2.3.2 Immunohistochemistry of CBP protein—Approximately 10 histological sections from each brain, spaced at 500 μm intervals and spanning the rostro-caudal extent of the hippocampus, were probed for CBP immunoreactivity. Material from animals representing all age and cognitive status conditions was included in every run of immunocytochemical processing. Free-floating sections were washed in Tris-buffered saline (TBS: 137mM NaCl, 3mM KCl, 25mM Tris, pH 7.4) with Tween-20 (TBST) and then blocked for 1 hr with 5% normal donkey serum in TBST. The tissue was incubated overnight with polyclonal anti-CBP primary antibody (CBP C-20, sc-583; Santa Cruz Biotechnology Inc., Santa Cruz, CA, USA), diluted 1:250 in 5% normal donkey serum and TBST. After two, 5-min washes with TBST and a 5-min wash with TBS, the tissue was incubated with fluorescent donkey anti-rabbit secondary antibody (Alexa Fluor® 594; Invitrogen, Carlsbad, CA, USA) diluted 1:200 in bovine serum albumin in TBS, for 2 hr. Starting with this step, all incubations and washes were performed in the dark. The sections were washed three times with TBST and twice with TBS, followed by a 3-min incubation with SYTOX® Green nucleic acid stain (Invitrogen) diluted 1:30,000 in TBS, in order to visualize cell nuclei. Finally, the sections were mounted onto glass slides, allowed to dry briefly and coverslipped with 2.5% PVA-DABCO solution in 0.1M Tris-HCl [(PVA: Polyvinyl alcohol), DABCO: 1,4-Diazabicyclo[2.2.2]octane; Sigma, St. Louis, MO, USA]. To confirm the specificity of the antibody, selected sections from representative Y, AU and AI brains were incubated with antibody that had been previously conjugated with CBP peptide (sc-583 peptide; Santa Cruz Biotechnology Inc.). No significant immunoreactivity was detected under these conditions.

2.3.3 Image collection and quantification—Fluorescence labeling in the histological sections was digitized on a Typhoon Trio^{+} Imaging system (GE Healthcare, Piscataway, NJ, USA). For CBP detection, the excitation laser was set at 532 nm, the emission filter was centered at 610 nm with a band-pass of 30 nm, and the photomultiplier was set at 520 V. SYTOX® Green excitation was set at 488 nm, the filter was centered at 520 nm with a band-pass of 40 nm and the photomultiplier tube was set at 475 V or 450 V, to account for run to run variability. Images were digitized at the highest available resolution with a pixel size of 10 μm. The acquired 16-bit gray scale images were then imported into ImageJ (http://rsbweb.nih.gov/ij/) and pseudo-colored using the “Fire” lookup table to facilitate the delineation of the regions of interest. Mean fluorescence intensity per animal was quantified along the entire septo-temporal axis of the hippocampus separately for the pyramidal cell layer of CA1, CA2/CA3, and the granular cell layer of the dentate gyrus (DG). Fluorescent signal intensity in CA1, CA2/CA3 and DG was normalized to whole section intensity, partially controlling for individual differences in overall labeling.

A subset of sections was also imaged on a Zeiss LSM710 (Carl Zeiss MicroImaging, LLC, Thornwood, NY, USA) laser-scanning confocal microscope. For this analysis, we quantified CBP immunostaining intensity in four sections per brain through the dorsal hippocampus in six animals per group. All sections were scanned using the same imaging parameters (Plan-Apochromat 20x/0.8n.a. objective; laser: 561nm, 5.0% intensity; pinhole: 39μm; master gain: 500; digital gain: 0; digital offset: 0). For each section and anatomical site (both left and right CA1, CA3 and DG), one z-stack composed of 8-bit images was collected. The images collected were 425 μm × 425 μm (0.415 μm/pixel), with a z-step of 1.052 μm. Immunofluorescence staining intensity for CBP was quantified using ZEN2008 image collection and analysis software (Carl Zeiss MicroImaging, LLC). Four contiguous scans

were selected through the z-axis of each image stack (avoiding the cut surfaces and yielding a 4.2 μm-tick homogeneously stained section), the pyramidal cell layer of CA1 or CA3, or the granular cell layer of the DG was delineated, and the threshold was adjusted in order to quantify predominantly intra-nuclear staining. Using this approach, immunofluorescent signal intensity was measured at high resolution in 32 sampling sites each for CA1, CA3 and DG per brain.

2.3.4 WND-CHARM algorithm for image analysis—In order to provide an independent, quantitative assay of observed immunohistochemical morphology as it related to age and cognitive ability, we took advantage of the WND-CHARM classification algorithm (Orlov, et al., 2008, http://code.google.com/p/wnd-charm) which uses supervised machine learning to assess the morphological distinctiveness of experimentally defined groups of images (Y, AU and AI in this analysis) indicated by classification accuracy. First, three digitized images representing the same approximate region of the dorsal hippocampus from each animal (n=11 for Y, n=9 for AU and n=11 for AI) were selected from among those collected on the Typhoon Trio$^+$ Imaging system (GE Healthcare). The images were cropped to a standard size (CA1 - 67×36 pixel, CA3 - 81×48 pixel, DG - 62×35 pixel) selecting the same approximate anatomical region of CA1, CA3 and DG, and rotated in order to normalize the orientation of the principal cell layer. These dimensions accommodated maximal area while holding the alignment of the cell body layers and other global anatomical features constant across images. By this approach, areas captured in the CA1 images included portions of *stratum oriens*, *stratum pyramidale*, and *stratum radiatum*; in CA3 they included *stratum oriens*, *stratum pyramidale*, *stratum lucidum*, and *stratum radiatum*; and DG images contained the polymorphic layer, *stratum granulosum*, and *stratum moleculare* (see Fig. S1).

WND-CHARM image classification analysis was conducted separately for each hippocampal sub-region and for CBP and SYTOX®Green labeling. For each group, 3 images per animal were used in the analysis (33 images for Y, 27 for AU and 33 for AI). The image classifier algorithm processed each image by first deriving additional representations of their pixel planes using image transforms that are common in signal processing (Fourier, Wavelet, Chebyshev, etc.) as well as transforms of transforms. These representations were run through a battery of general-purpose image assays (polynomial decompositions, high contrast features, pixel statistics and texture measurements) resulting in a vector of 2873 features describing each image. These features were rank ordered based on their ability to discriminate the three image classes (Y, AU and AI), and only the top 15% (433 features) representing the highest signal-to-noise ratio were used in classification. Classification accuracy was calculated for each hippocampal sub-region and fluorescent label based on 5,000 iterations of randomized train/test splits. Each iteration involved randomly dividing the pool of 93 total images into three sets: 66 images (22Y, 22AU and 22 AI) were used to train the classifier, 15 images (5Y, 5AU and 5AI) were used for testing, and 12 images (6Y and 6AI) were held in reserve to ensure a balanced design across groups. Finally, 95% confidence intervals were calculated using the normal approximation of the binomial distribution. Using this design, the classification accuracy results reflect a total of 75,000 images sorted.

2.4 Western Blot

2.4.1 Tissue collection—A separate set of animals was used to quantify hippocampal CBP protein by western blot analysis. Animals (6Y, 6AU and 8AI) were sacrificed a minimum of two weeks after behavioral characterization, by decapitation directly from the home cage (the same delay was used for all age groups). The brain was quickly removed, the hippocampus was isolated, and the CA1, CA3 and DG subfields were micro-dissected on

an ice-chilled glass plate under a stereomicroscope. The tissue was homogenized in hypotonic buffer [10 mM HEPES, 1.5 mM $MgCl_2$, 10 mM KCl and 2X Protease Inhibitor (Thermo Scientific, Rockford, IL, USA)] and incubated on ice for 30 min. The solution was lysed with a syringe and incubated on ice for 15 min, followed by centrifugation at 4°C for 15 min at 1000*g*. The supernatant (cytosolic fraction) was removed and the nuclear pellet was resuspended in hypotonic buffer and centrifuged at 1000*g* for 15 min at 4°C. Finally, the pellet was resuspended in 5% SDS and stored at −80°C.

2.4.2 Immunoblotting—The concentration of the samples was determined using the Bicinchoninic acid (BCA) protein assay (Thermo Scientific) followed by dilution with water, normalizing for total loaded protein. Material was separated by sodium dodecyl sulfate polyacrylamide gel electrophoresis (SDS-PAGE) in a 3–8% Tris-Acetate gel (Invitrogen) and the proteins transferred to a transfer membrane using the iBlot system (Invitrogen). The membrane was incubated with blocking solution [2% ECL advance blocking agent (GE Healthcare) in PBS with 0.1% Tween-20 (PBST)] for 1 hr at room temperature. After two 5-min washes in PBST, membranes were incubated overnight with primary antibodies, at room temperature, with shaking. The CBP antibody (CBP A-22, sc-369; Santa Cruz Biotechnology Inc.) was diluted 1:200 in blocking buffer and β-actin (BioVision, Mountain View, CA, USA), used as a protein loading control, was diluted at 1:1000. Membranes were washed in PBST and incubated with Alexa Fluor®488 and Alexa Fluor®633 conjugated secondary antibodies (Invitrogen) diluted 1:2500 in PBST, at room temperature for 1 hr with shaking, and protected from light. The membrane was washed again in PBST, followed by a final wash in PBS and allowed to dry. Membranes were scanned at a resolution of 100μm/pixel on a Typhoon Trio$^+$ Imaging system (GE Healthcare) and fluorescent bands were quantified using ImageQuant TL image analysis software (GE Healthcare). Peptide competition assays were conducted by incubating excess peptide (sc-369P; Santa Cruz Biotechnology Inc.) with the primary antibody before use. These assays showed no band at the appropriate molecular weight for CBP, confirming the specificity of the antibody.

2.5 Statistical analysis

Statistical analysis was conducted using SPSS (PASW Statistics, version 18.0, IBM, Chicago, IL, USA) running under Mac OS X (version 10.6.6, Apple, Cupertino, CA, USA). For the immunocytochemistry measures, a repeated measures ANOVA was performed with age and cognitive status as between-subject variables, and hippocampal subfield as the within-subject measure. For the immunoblots, a univariate ANOVA was carried out, testing for potential differences among the Y, AU and AI groups. The microdissected hippocampal subfields were processed separately in this analysis, preventing direct comparisons across anatomical regions. Two-tailed Pearson r correlation coefficients were computed between the learning index scores from behavioral testing and: 1) the CBP immunoreactivity intensity values, and 2) CBP protein levels quantified by western blotting. All data are summarized as mean ± standard error of the mean, except for the WND-CHARM classification accuracy, for which we used 95% confidence intervals based on the normal approximations of the binomial distribution.

3. Results

3.1 Behavioral characterization

The results of behavioral testing were similar to previous studies in this model of normal cognitive aging (Gallagher, et al., 2003, Haberman, et al., 2009, Smith, et al., 2000). The learning index (LI) scores for the individual subjects in the immunohistochemical experiment are shown in Fig. 1A, with scores ranging in young animals (Y) from 153.6 to

236.7 (average 203.1±9.7, n=11). Adopting a strategy validated in Gallagher, et al. (1993) and elsewhere (Gallagher, et al., 2003, Haberman, et al., 2009, Smith, et al., 2000), aged animals with LI values overlapping Y rats were classified as aged unimpaired (AU, range = 184.9 to 243.0; average 212.8±6.9, n=9), and the remainder were designated aged impaired (AI, LI range = 257.9 to 327.0; average 289.8±6.3, n=11). The LI scores for the individual subjects used in the western blotting experiment are shown in Fig. 1B. In Y animals, scores ranged from 193.2 to 239.0, averaging 211.5±7.9 (n=6), in AU animals, the scores ranged from 211.9 to 233.3, averaging 221.0±3.6 (n=6), while in AI animals, LI scores ranged from 242.5 to 305.6, averaging 279.8±8.0 (n=8).

3.2 Hippocampal CBP immunofluorescence is preserved during cognitive aging

Male Long-Evans rats were sacrificed directly from the home cage and the brains were processed for the immunocytochemical visualization of CBP, providing a window on baseline availability of this transcription factor with HAT activity. SYTOX®Green nucleic acid counterstain was used to control for cell packing density. Qualitative assessment confirmed that all hippocampal fields presented immunoreactivity, with intensity varying approximately with cell packing density. Quality and overall staining characteristics were subjectively similar in the young and aged material. Mean CBP immunoreactivity in the CA1 pyramidal cell layer normalized to whole section intensity was 1.19±0.01 in the Y group (n=11), 1.20±0.01 in AU (n=9) and 1.20±0.01 in AI rats (n=11). Across the CA2/CA3 pyramidal cell layer, CBP immunoreactivity averaged 1.19±0.01, 1.19±0.01 and 1.21±0.01 in the Y, AU and AI groups, respectively. In the granule cell layer of the DG, normalized CBP intensity was 1.34±0.01 in Y, 1.33±0.02 in AU and 1.35±0.01 in AI. A repeated measures ANOVA showed no interaction between group and hippocampal region (F[4,56]=0.9, p=0.48), and confirmed that CBP immunostaining intensity was statistically equivalent across groups (main effect of group F[2,28]=1.2, p=0.33) (Fig. 2A,C). This analysis additionally revealed a statistically significant main effect of hippocampal region (F[2,56]=726.6, p<0.01), and follow-up pairwise tests using the Bonferroni adjustment for multiple comparisons showed that CBP staining intensity was significantly higher in the DG granule cell layer than in either the pyramidal cell layer of CA1 (p<0.01) or CA2/CA3 (p<0.01). The comparison between the pyramidal cell layers of CA1 and CA2/CA3 did not yield statistically significant differences (p=1.00). These findings are important because they confirm that the quantitative methods used here were sufficiently sensitive to detect relatively subtle regional differences in intensity of CBP immunofluorescence staining.

Brain volume can decline during normal aging (Driscoll, et al., 2006) in the absence of significant neuron loss (Rapp and Gallagher, 1996). In the present experiments we therefore used SYTOX®Green nucleic acid stain to label cell nuclei and test for the possible influence of age-related changes in cell packing density. Intensity values, normalized to whole section intensity were similar across groups. In the CA1 subfield of the hippocampus SYTOX®Green intensity was 1.17±0.04, 1.15±0.06 and 1.14±0.04 for the Y, AU and AI groups, respectively. Corresponding values for the CA3 pyramidal cell layer were 1.05±0.01 for Y, 1.04±0.01 for AU, and 1.04±0.01 for group AI. In the DG granule cell layer, fluorescence levels were 1.73±0.02 for Y, 1.67±0.04 for AU and 1.69±0.02 for AI (Fig. 2B,D). A repeated measures ANOVA showed no interaction between group and hippocampal region (F[4,56]=0.2, p=0.94), and confirmed that labeling intensity was equivalent across groups (F[2,28]=1.1, p=0.33), indicating that age-dependent change in general cytological organization of the hippocampus is unlikely masking alterations in CBP staining intensity. Similar to CBP immunolabeling, there was a significant main effect of hippocampal region (F[2,56]=244.6, p<0.01), with pairwise comparisons revealing significant differences with higher intensity values in DG than CA1 (p<0.01) and CA2/CA3 (p<0.01), and higher intensity values in CA1 than in CA2/CA3 (p=0.01).

Previous studies have provided evidence for differential roles of the dorsal and ventral hippocampus in memory (for review, see Fanselow and Dong, 2010). In order to test for potential regional selectivity in the effects of aging on CBP immunoreactivity, we analyzed fluorescent intensity separately in sections that contained dorsal hippocampus only (anterior; approximately two thirds of the total number of hippocampal sections analyzed), and in sections containing both dorsal and ventral hippocampus (posterior; approximately one third of the total number of hippocampal sections analyzed). A repeated measures ANOVA revealed no statistically significant triple interaction between cognitive aging, anterio-posterior axis and hippocampal region (F[4,56]=0.2, p=0.94, Fig. 2E). The interaction between antero-posterior level and cognitive status also failed to reach statistical significance (F[2,28]=2.6, p=0.09), but there was a significant interaction between hippocampal region and antero-posterior axis (F[2,56]=53.6, p<0.01). We also found a reliable main effect of antero-posterior subdivision (F[1,28]=117.3, p<0.01), with sections containing only dorsal hippocampus displaying greater CBP immunofluorescence intensity than more posterior sections (1.26±0.01 versus 1.22±0.01, respectively). To further analyze this regional difference, for each hippocampal subfield we performed a repeated measures ANOVA with antero-posterior subdivision as the within-subject variable, and chronological age/cognitive status as a between subject factor. The results revealed no significant interaction between the two variables for any of the principal cell layers (F[2,28]=1.5, p=0.24 for CA1, F[2,28]=1.7, p=0.21 for CA3 and F[2,28]=1.1, p=0.34 for DG), but a significant effect of antero-posterior axis for CA1 (F[1,28]=306.9, p<0.01) and DG (F[1,28]=61.1, p<0.01), with the anterior region showing higher CBP immunoreactivity than the posterior division. In CA3 there was no effect of dorsoventral level (F[1,28]=1.2, p=0.29). These results are consistent with evidence for anatomical differentiation along the dorsoventral axis of the hippocampus (Fanselow and Dong, 2010). It might also be, however, that a systematic change in the preferred orientation of principal cells, relative to the fixed plane of section, contributes to these observations. In either case, the results reinforce the conclusion that the quantitative methods used here can detect even relatively subtle differences in immunoreactivity. Against this background, the absence of effects on CBP staining intensity in relation to age and cognitive status is striking.

Correlation statistics tested the possibility that individual variability in spatial learning ability is associated with baseline, resting levels of CBP. Correlations between CBP immunoreactivity intensity and learning index (LI) scores were computed for each hippocampal region separately (Fig. 3). No statistically significant correlations were found when Y, AU and AI rats were considered separately, when the results were combined across the aged subjects (i.e., AU+AI), or when all animals were considered together in the analysis (Table 1). However, it is worth noting that numerically, the strongest correlation involved CA2/CA3 (r=0.33, p=0.07 for all animals, r=0.39, p=0.09 considering aged animals only), the same hippocampal subfield that gene expression data (Haberman, et al., 2009) and *in vivo* electrophysiology studies (Wilson, et al., 2005) have shown to be most closely linked to spatial learning impairment in this animal model.

Taken as a whole, the results suggest that CBP levels in the hippocampus remain stable as a function of chronological and cognitive aging.

3.3 High resolution quantitative confocal microscopy confirms the stability of hippocampal CBP immunoreactivity in normal cognitive aging

Next we sought to confirm our initial findings by an independent approach, using confocal microscopy to analyze a subset of the immunolabeled sections. As can be seen in Fig. 4A, CBP immunolabeling was localized to cell nuclei and present in essentially all neurons. By analyzing the tissue at sub-micron resolution, it was possible to virtually eliminate the contribution of background fluorescence and restrict the quantification of CBP

immunoreactivity to nuclear label. For this analysis, a representative sample of six animals from each group was selected with average intensity values, as determined by the initial lower resolution imaging, within one standard deviation of the overall mean. Four histological sections from each brain were examined, and both left and right dorsal hippocampi were analyzed. Using ZEN2008® image analysis software, CBP nuclear immunofluorescence intensity was quantified in a total of 32 images from each hippocampal subfield in each animal (Carl Zeiss MicroImaging, LLC). Mean values for the CA1 pyramidal cell layer were 76.7±2.9 in group Y, 83.7±3.5 in AU and 76.4±2.0 in AI. In CA3 pyramidal neurons, CBP staining intensity averaged 79.1±1.8 in Y, 78.4±2.6 in AU and 80.2±2.6 in group AI. Corresponding values for the granule cell layer of the DG were 95.3±3.6, 108.1±5.9, and 99.1±4.0 in the Y, AU, and AI groups, respectively (Fig. 4B).

A repeated measures ANOVA showed a highly significant difference across hippocampal area ($F[2,30]=159.4$, $p<0.01$), but no statistically significant effect of cognitive status or age on CBP intensity ($F[2,15]=1.1$, $p=0.35$). Bonferroni post hoc analysis revealed that the significant hippocampal area effect was due to higher CBP staining intensity in the DG granule cell layer compared with either CA1 ($p<0.01$) or CA3 pyramidal cells ($p<0.01$). The CA1 and CA3 comparison did not show a significant difference ($p=1.00$). This analysis also revealed a statistically significant interaction between cognitive status and hippocampal area ($F[4,30]=4.7$, $p<0.01$), presumably reflecting the numerically higher intensity observed selectively in the CA1 and DG, but not in the CA3, of AU animals (see Fig. 4B). However, independent one-way ANOVAs, performed *a posteriori* did not reveal significant differences across groups distinguished by cognitive status (CA1: $F[2,15]=2.1$, $p=0.16$; CA3: $F[2,15]=0.1$, $p=0.86$; DG: $F[2,15]=2.0$, $p=0.17$). These results suggest that CBP protein content is greater among granule cell nuclei than in other principal neurons of the hippocampus, and that these levels are unchanged as a consequence of normal cognitive aging.

3.4 WND-CHARM image analysis shows above chance accuracy at classifying dentate gyrus and CA3 images, independent of CBP levels

Next we took advantage of yet another independent approach that, in generic form, considers thousands of imaging parameters in exemplar training images as a basis for the capacity to then classify new items according to group identity (Y, AU and AI in the present case). Sensitivity of the approach in the context of aging has been validated in a study in *Caenorhabditis elegans* documenting structural transitions in skeletal muscle (Johnston, et al., 2008). The classification algorithm takes into account not only staining intensity, but also spatial distribution and many other imaging attributes and mathematical transforms (Orlov, et al., 2008). This analysis was performed on images selected from among those collected on the Typhoon Trio$^+$ Imaging system (GE Healthcare). The images were cropped to a fixed size and represented the same approximate cross-sectional area in each hippocampal field. This ensured that observed effects reflect intrinsic properties of the histological preparations and are not a consequence of systematic differences in how the images for the different groups were formatted. For representative images used see Fig. S1.

Results from the WND-CHARM algorithm analysis are summarized in Table 2. The algorithm's accuracy in sorting images was significantly above chance (i.e., 33.3%) for CBP (42.2 ± 0.4 %) and SYTOX®Green staining (48.9 ± 0.4 %) in the DG, and for SYTOX®Green alone in CA3 (49.2 ± 0.4 %). Since we found above chance classification for both markers in the DG, we followed up the analysis with two-way comparisons between Y and A, and between AU and AI animals. Correct classification was higher for the AU vs. AI comparison for both CBP (62.5 ± 0.4 %) and SYTOX®Green (68.5 ± 0.4 %) than for the Y vs. A comparison − 55.8 ± 0.4% and 56.5 ± 0.4% respectively (since these are two-way comparisons, chance accuracy is 50 %). It is important to note that the accuracy values were

relatively modest and that the only significant reliable classification observed for CBP immunolabeling (i.e., in DG) was accompanied by a similar result for the paired SYTOX®Green labeled images. This pattern of results therefore suggests that the differences enabling correct classification are unrelated to CBP immunoreactivity specifically, and instead involve other features of the aged DG. At the same time, because the factors driving the image classification are derived from transforms of the original images, it is not possible to relate the DG features that differ in young and aged animals to standard neuroanatomical parameters such as size, shape and orientation. A list of the top 50 features responsible for the algorithm's above chance classification is provided in Tables S1–S3.

3.5 Hippocampal CBP protein quantified by western blot is maintained with age and cognitive status

In a final analysis we quantified CBP protein levels in microdissected samples of CA1, CA3 and DG by western blot using an antibody directed against a different CBP epitope than in the histological analyses. Hippocampal subfields were processed separately, and accordingly, a univariate ANOVA was computed for each. No statistically significant differences were found between groups (CA1: $F[2,17]=0.7$, $p=0.53$; CA3: $F[2,17]=1.0$, $p=0.38$; DG: $F[2,17]=0.8$, $p=0.46$, Fig. 5). Similar to the immunohistochemistry results, hippocampal CPB protein levels measured by western blot failed to reveal significant correlations with the learning index scores for either cognitive status, age, or collapsed across conditions (see Table 3). These findings independently confirm the outcome of the histological and image classifier analyses, supporting the conclusion that baseline levels of hippocampal CBP remain stable with age and cognitive status.

4. Discussion

The present experiments tested the hypothesis that CBP protein levels in the hippocampus are coupled with individual differences in spatial learning capacity in a rat model of normal cognitive aging. In summary, our results indicate that under baseline conditions, constitutive hippocampal CBP immunoreactivity does not vary in relation to age or cognitive status in male Long-Evans rats. Stability was documented independently by multiple techniques including Western blot, quantification of regional immunofluorescence intensity at both low and high cellular resolution, and by automated digital image classifier analysis. Importantly, the quantitative methods used here proved sufficiently sensitive to detect other, relatively modest differences in the same material. Our results revealed elevated CBP immunolabeling in sections through anterior levels, where only the dorsal hippocampus is present, compared to more posterior sections that included both dorsal and ventral aspects. Although this difference might relate to functional specialization along the antero-posterior axis (Fanselow and Dong, 2010), the contribution of other factors, including dorsoventral changes in the preferred orientation of the principal neurons, cannot be excluded. CBP labeling also varied reliably across the principal cell fields of the hippocampus, with the DG displaying higher levels of CBP than either CA1 or CA3. Although this effect may arise partly from differences in neuronal packing density, the observation that a similar pattern is observed when labeling is quantified in single cells by confocal microscopy suggests that intensity of CBP labeling may be higher in granule cell nuclei. The smaller size of granule cell nuclei relative to pyramidal neurons (Kraszpulski, et al., 1996, Walsh and Cummins, 1979) may contribute to this result by concentrating CBP protein in a smaller volume. Finally, the WND-CHARM image analysis algorithm displayed better than chance accuracy at classifying DG images from all groups. This differential classification was not specific to CBP labeling, however, since equivalent classification accuracy was achieved in the same tissue counterstained with SYTOX®Green. The features that enabled correct classification are mathematical transforms derived from digital image files, and are not easily related to

standard cytological features examined in conventional image analysis. Indeed an informal, subjective survey of the available images revealed no distinguishing characteristics of the aged hippocampus for any field, including the DG. The vulnerability of the DG documented here could arise from subtle alterations in architectural organization, such as the loss of axospinous synapses reported by Geinisman, et al. (1992), or as consequence of more dynamic changes of the sort responsible for the cerebral blood volume decrease observed in aged monkeys (Small, et al., 2004).

The study of epigenetics in the context of learning and memory has received increased attention in recent years, implicating a variety of epigenetic modifications in memory-related synaptic plasticity (for reviews, see Barrett and Wood, 2008, Gräff and Mansuy, 2008, Levenson and Sweatt, 2005). Current evidence raises the possibility that epigenetic mechanisms may also contribute to the learning and memory deficits observed during normal and pathological aging (Gravina and Vijg, 2010, Penner, et al., 2010, Zeng, et al., 2011). As a transcription factor with histone acetylation activity (Ogryzko, et al., 1996), CBP is positioned to play a key modulatory role. Noteworthy findings in this context demonstrate that, in *C. elegans,* increased longevity induced by dietary restriction is prevented by cbp-1 RNAi administration (Zhang, et al., 2009). The same study also found that CBP mRNA levels in the hypothalamus are positively correlated with lifespan across five strains of mice. More recently, Peleg, et al. (2010) reported that hippocampal baseline CBP mRNA and protein are similar between 3 and 16 month-old mice. In that study, however, there was a numerical increase after fear conditioning in CPB mRNA in 3 but not 16 month-old animals (protein levels were not reported). In contrast to the present findings in Long-Evans rats, Chung, et al. (2002) previously described a marked decrease in CBP immunoreactivity in both hippocampus and neocortex of aged Sprague-Dawley rats relative to young adults. Thus, aside from potential strain differences, one way of accommodating the available findings is to suppose that uncontrolled environmental events prior to sacrifice (e.g., animal colony activity) might have induced CBP expression in young but not aged rats. Another study in the Sprague-Dawley model mapped the anatomical distribution of CBP immunoreactivity in the adult rat brain (Strömberg, et al., 1999) using a protocol similar to Chung, et al. (2002). Staining varied substantially not only across brains, but also within anatomical structures across hemispheres. Immunocytochemical labeling in the present analysis was qualitatively quite consistent, and it seems reasonable to speculate that less optimal, more variable staining might give rise to an apparent decline when CBP-positive cell density is measured. Using a battery of independent approaches, however, we report an absence of association between baseline levels of CBP in the hippocampus and cognitive or chronological age.

The cell biological and molecular mechanisms underlying normal and pathological forms of cognitive aging appear distinct (Morrison and Hof, 2002). Several previous reports have implicated histone acetylation and CBP levels in the pathology of Alzheimer's disease. Kilgore, et al. (2010), for example, demonstrated that memory deficits in the APPswe/PS1dE9 double-transgenic mouse model are reversed by HDAC1 inhibitor administration. CBP protein expression is decreased in a forebrain-specific double presenilin conditional knockout mouse (Saura, et al., 2004), and in flies, CBP levels in the central nervous system are reduced in the absence of presenilin (Boyles, et al., 2010). Furthermore, Rouaux, et al. (2003) and Saha, et al. (2009) found that CBP levels are decreased during neuronal apoptosis and that increasing expression can protect against toxic insults. Together, these studies implicate CBP in neurodegeneration and cellular dysfunction. By this perspective, and in contrast to the substantial neuronal preservation seen during normal aging (Rapp and Gallagher, 1996, Rasmussen, et al., 1996), changes in CBP levels may be particularly relevant in conditions of age-related neurodegenerative disease.

Activity of CBP can be modulated through a variety of processes. Liu, et al. (1998) first described transcriptional activation of CBP in cell culture by cAMP through PKA activity, and by NGF through the MAPK pathway. CBP levels can also be modulated in vivo by behavior and a recently published study from our laboratory reported that hippocampal CBP protein levels are reduced equivalently in Y, AU and AI animals, 2 hours following behavioral activation in a modified version of the Morris water maze (Castellano, et al., 2012). The direction of this effect was unexpected, but may reveal a complex pattern of temporally regulated changes in experience-dependent CBP dynamics. Aside from changes in protein levels, phosphorylation of CBP can influence the expression of downstream genes (Huang, et al., 2007, Impey, et al., 2002). While the specific mechanisms are still being unveiled (Xia, et al., 2011), current evidence indicates that phosphorylation at different sites can either up- or down-regulate CBP mediated HAT activity (Ait-Si-Ali, et al., 1999, Hong, et al., 2002). What remains to be more fully explored is whether cognitive aging is accompanied by temporally and regionally specific changes in the dynamic modulation of CBP in response to recent experience.

Supplementary Material

Refer to Web version on PubMed Central for supplementary material.

Acknowledgments

We thank Robert McMahan, Dr. James Castellano and Dr. Bonnie Fletcher for technical support and the members of the Neurocognitive Aging Section of the Laboratory of Experimental Gerontology for helpful discussions. This research was supported by the Intramural Research Program of the National Institute on Aging; by NIH grant AG09973; and by Fundação para a Ciência e a Tecnologia grant SFRH/BD/27758/2006.

References

Ait-Si-Ali S, Carlisi D, Ramirez S, Upegui-Gonzalez LC, Duquet A, Robin P, Rudkin B, Harel-Bellan A, Trouche D. Phosphorylation by p44 MAP Kinase/ERK1 stimulates CBP histone acetyl transferase activity in vitro. Biochemical and Biophysical Research Communications. 1999; 262(1): 157–62. [PubMed: 10448085]

Alarcón JM, Malleret G, Touzani K, Vronskaya S, Ishii S, Kandel ER, Barco A. Chromatin acetylation, memory, and LTP are impaired in CBP+/− mice: a model for the cognitive deficit in Rubinstein-Taybi syndrome and its amelioration. Neuron. 2004; 42(6):947–59. [PubMed: 15207239]

Barrett R, Wood M. Beyond transcription factors: the role of chromatin modifying enzymes in regulating transcription required for memory. Learning & Memory. 2008; 15(7):460–7. [PubMed: 18583646]

Bourtchouladze R, Lidge R, Catapano R, Stanley J, Gossweiler S, Romashko D, Scott R, Tully T. A mouse model of Rubinstein-Taybi syndrome: defective long-term memory is ameliorated by inhibitors of phosphodiesterase 4. Proceedings of the National Academy of Sciences of the United States of America. 2003; 100(18):10518–22. [PubMed: 12930888]

Bousiges O, Vasconcelos APd, Neidl R, Cosquer B, Herbeaux K, Panteleeva I, Loeffler JP, Cassel JC, Boutillier AL. Spatial memory consolidation is associated with induction of several lysine-acetyltransferase (histone acetyltransferase) expression levels and H2B/H4 acetylation-dependent transcriptional events in the rat hippocampus. Neuropsychopharmacology. 2010; 35(13):2521–37. [PubMed: 20811339]

Boyles RS, Lantz KM, Poertner S, Georges SJ, Andres AJ. Presenilin controls CBP levels in the adult Drosophila central nervous system. PLoS One. 2010; 5(12):e14332. [PubMed: 21179466]

Castellano JF, Fletcher BR, Kelley-Bell B, Kim DH, Gallagher M, Rapp PR. Age-related memory impairment is associated with disrupted multivariate epigenetic coordination in the hippocampus. PLoS One. 2012; 7(3):e33249. [PubMed: 22438904]

Chen G, Zou X, Watanabe H, van Deursen JM, Shen J. CREB binding protein is required for both short-term and long-term memory formation. The Journal of Neuroscience. 2010; 30(39):13066–77. [PubMed: 20881124]

Chung Y, Kim E, Shin C, Joo K, Kim M, Woo H, Cha C. Age-related changes in CREB binding protein immunoreactivity in the cerebral cortex and hippocampus of rats. Brain Research. 2002; 956(2):312–8. [PubMed: 12445700]

Driscoll I, Howard SR, Stone JC, Monfils MH, Tomanek B, Brooks WM, Sutherland RJ. The aging hippocampus: a multi-level analysis in the rat. Neuroscience. 2006; 139(4):1173–85. [PubMed: 16564634]

Fanselow MS, Dong HW. Are the dorsal and ventral hippocampus functionally distinct structures? Neuron. 2010; 65(1):7–19. [PubMed: 20152109]

Fletcher, BR.; Rapp, PR. Normal cognitive aging. In: Nelson, RJ.; Mizumori, SJY.; Wiener, IB., editors. Handbook of Psychology: Behavioral Neuroscience. Vol. 3. John Wiley & Sons, Inc; New York: 2012.

Gallagher M, Bizon J, Hoyt E, Helm K, Lund P. Effects of aging on the hippocampal formation in a naturally occurring animal model of mild cognitive impairment. Experimental Gerontology. 2003; 38(1–2):71–7. [PubMed: 12543263]

Gallagher M, Burwell RD, Burchinal MR. Severity of spatial learning impairment in aging: development of a learning index for performance in the Morris water maze. Behavioral Neuroscience. 1993; 107(4):618–26. [PubMed: 8397866]

Geinisman Y, deToledo-Morrell L, Morrell F, Persina IS, Rossi M. Age-related loss of axospinous synapses formed by two afferent systems in the rat dentate gyrus as revealed by the unbiased stereological dissector technique. Hippocampus. 1992; 2(4):437–44. [PubMed: 1308200]

Gräff, J.; Mansuy, I. Behavioural Brain Research. 2008. Epigenetic codes in cognition and behaviour.

Gravina S, Vijg J. Epigenetic factors in aging and longevity. Pflügers Archiv: European Journal of Physiology. 2010; 459(2):247–58.

Haberman RP, Colantuoni C, Stocker AM, Schmidt AC, Pedersen JT, Gallagher M. Prominent hippocampal CA3 gene expression profile in neurocognitive aging. Neurobiology of Aging. 2009

Hong W, Kim AY, Ky S, Rakowski C, Seo SB, Chakravarti D, Atchison M, Blobel GA. Inhibition of CBP-mediated protein acetylation by the Ets family oncoprotein PU.1. Molecular and Cellular Biology. 2002; 22(11):3729–43. [PubMed: 11997509]

Huang WC, Ju TK, Hung MC, Chen CC. Phosphorylation of CBP by IKKalpha promotes cell growth by switching the binding preference of CBP from p53 to NF-kappaB. Molecular Cell. 2007; 26(1): 75–87. [PubMed: 17434128]

Impey S, Fong AL, Wang Y, Cardinaux JR, Fass DM, Obrietan K, Wayman GA, Storm DR, Soderling TR, Goodman RH. Phosphorylation of CBP mediates transcriptional activation by neural activity and CaM kinase IV. Neuron. 2002; 34(2):235–44. [PubMed: 11970865]

Johnston J, Iser WB, Chow DK, Goldberg IG, Wolkow CA. Quantitative image analysis reveals distinct structural transitions during aging in Caenorhabditis elegans tissues. PLoS One. 2008; 3(7):e2821. [PubMed: 18665238]

Kilgore M, Miller CA, Fass DM, Hennig KM, Haggarty SJ, Sweatt JD, Rumbaugh G. Inhibitors of class 1 histone deacetylases reverse contextual memory deficits in a mouse model of Alzheimer's disease. Neuropsychopharmacology. 2010; 35(4):870–80. [PubMed: 20010553]

Korzus E, Rosenfeld M, Mayford M. CBP histone acetyltransferase activity is a critical component of memory consolidation. Neuron. 2004; 42(6):961–72. [PubMed: 15207240]

Kraszpulski M, Zawrocka-Wrzo kowa T, Lukaszyk I. Morphometrical study of rat hippocampus. Light-microscopic features. Folia Neuropathologica. 1996; 34(3):137–41. [PubMed: 8946785]

Levenson J, Sweatt J. Epigenetic mechanisms in memory formation. Nature Reviews Neuroscience. 2005; 6(2):108–18.

Levenson JM, O'Riordan KJ, Brown KD, Trinh MA, Molfese DL, Sweatt JD. Regulation of histone acetylation during memory formation in the hippocampus. The Journal of Biological Chemistry. 2004; 279(39):40545–59. [PubMed: 15273246]

Liu YZ, Chrivia JC, Latchman DS. Nerve growth factor up-regulates the transcriptional activity of CBP through activation of the p42/p44(MAPK) cascade. The Journal of Biological Chemistry. 1998; 273(49):32400–7. [PubMed: 9829969]

Morrison JH, Hof PR. Selective vulnerability of corticocortical and hippocampal circuits in aging and Alzheimer's disease. Progress in Brain Research. 2002; 136:467–86. [PubMed: 12143403]

Nyffeler M, Zhang WN, Feldon J, Knuesel I. Differential expression of PSD proteins in age-related spatial learning impairments. Neurobiology of Aging. 2007; 28(1):143–55. [PubMed: 16386336]

Ogryzko VV, Schiltz RL, Russanova V, Howard BH, Nakatani Y. The transcriptional coactivators p300 and CBP are histone acetyltransferases. Cell. 1996; 87(5):953–9. [PubMed: 8945521]

Oike Y, Hata A, Mamiya T, Kaname T, Noda Y, Suzuki M, Yasue H, Nabeshima T, Araki K, Yamamura K-i. Truncated CBP protein leads to classical Rubinstein-Taybi syndrome phenotypes in mice: implications for a dominant-negative mechanism. Human Molecular Genetics. 1999; 8(3): 387–96. [PubMed: 9949198]

Orlov N, Shamir L, Macura T, Johnston J, Eckley DM, Goldberg IG. WND-CHARM: Multi-purpose image classification using compound image transforms. Pattern Recognition Letters. 2008; 29(11): 1684–93. [PubMed: 18958301]

Peleg S, Sananbenesi F, Zovoilis A, Burkhardt S, Bahari-Javan S, Agis-Balboa RC, Cota P, Wittnam JL, Gogol-Doering A, Opitz L, Salinas-Riester G, Dettenhofer M, Kang H, Farinelli L, Chen W, Fischer A. Altered histone acetylation is associated with age-dependent memory impairment in mice. Science. 2010; 328(5979):753–6. [PubMed: 20448184]

Penner MR, Roth TL, Barnes CA, Sweatt JD. An epigenetic hypothesis of aging-related cognitive dysfunction. Frontiers in Aging Neuroscience. 2010; 2:9. [PubMed: 20552047]

Petrij F, Giles RH, Dauwerse HG, Saris JJ, Hennekam RC, Masuno M, Tommerup N, van Ommen GJB, Goodman RH, Peters DJ, HBM. Rubinstein-Taybi syndrome caused by mutations in the transcriptional co-activator CBP. Nature. 1995; 376(6538):348–51. [PubMed: 7630403]

Rapp PR, Gallagher M. Preserved neuron number in the hippocampus of aged rats with spatial learning deficits. Proceedings of the National Academy of Sciences of the United States of America. 1996; 93(18):9926–30. [PubMed: 8790433]

Rasmussen T, Schliemann T, Sørensen JC, Zimmer J, West MJ. Memory impaired aged rats: no loss of principal hippocampal and subicular neurons. Neurobiology of Aging. 1996; 17(1):143–7. [PubMed: 8786797]

Rosenzweig E, Barnes C. Impact of aging on hippocampal function: plasticity, network dynamics, and cognition. Progress in Neurobiology. 2003; 69(3):143–79. [PubMed: 12758108]

Rouaux C, Jokic N, Mbebi C, Boutillier S, Loeffler JP, Boutillier AL. Critical loss of CBP/p300 histone acetylase activity by caspase-6 during neurodegeneration. The EMBO Journal. 2003; 22(24):6537–49. [PubMed: 14657026]

Rowe W, Blalock E, Chen KC, Kadish I, Wang D, Barrett J, Thibault O, Porter N, Rose G, Landfield P. Hippocampal expression analyses reveal selective association of immediate-early, neuroenergetic, and myelinogenic pathways with cognitive impairment in aged rats. The Journal of Neuroscience. 2007; 27(12):3098–110. [PubMed: 17376971]

Saha RN, Ghosh A, Palencia CA, Fung YK, Dudek SM, Pahan K. TNF-alpha preconditioning protects neurons via neuron-specific up-regulation of CREB-binding protein. Journal of Immunology. 2009; 183(3):2068–78.

Saura CA, Choi SY, Beglopoulos V, Malkani S, Zhang D, Shankaranarayana Rao BS, Chattarji S, Kelleher RJ, Kandel ER, Duff K, Kirkwood A, Shen J. Loss of presenilin function causes impairments of memory and synaptic plasticity followed by age-dependent neurodegeneration. Neuron. 2004; 42(1):23–36. [PubMed: 15066262]

Small SA, Chawla MK, Buonocore M, Rapp PR, Barnes CA. Imaging correlates of brain function in monkeys and rats isolates a hippocampal subregion differentially vulnerable to aging. Proceedings of the National Academy of Sciences of the United States of America. 2004; 101(18):7181–6. [PubMed: 15118105]

Smith TD, Adams MM, Gallagher M, Morrison JH, Rapp PR. Circuit-specific alterations in hippocampal synaptophysin immunoreactivity predict spatial learning impairment in aged rats. The Journal of Neuroscience. 2000; 20(17):6587–93. [PubMed: 10964964]

Stefanko D, Barrett R, Ly A, Reolon G, Wood M. Modulation of long-term memory for object recognition via HDAC inhibition. Proceedings of the National Academy of Sciences of the United States of America. 2009; 106(23):9447–52. [PubMed: 19470462]

Strömberg H, Svensson SPS, Hermanson O. Distribution of CREB-binding protein immunoreactivity in the adult rat brain. Brain Research. 1999; 818(2):510–4. [PubMed: 10082838]

Valor LM, Pulopulos MM, Jimenez-Minchan M, Olivares R, Lutz B, Barco A. Ablation of CBP in forebrain principal neurons causes modest memory and transcriptional defects and a dramatic reduction of histone acetylation but does not affect cell viability. The Journal of Neuroscience. 2011; 31(5):1652–63. [PubMed: 21289174]

VanGuilder HD, Yan H, Farley JA, Sonntag WE, Freeman WM. Aging alters the expression of neurotransmission-regulating proteins in the hippocampal synaptoproteome. Journal of Neurochemistry. 2010; 113(6):1577–88. [PubMed: 20374424]

Walsh RN, Cummins RA. Changes in hippocampal neuronal nuclei in response to environmental stimulation. The International Journal of Neuroscience. 1979; 9(4):209–12. [PubMed: 489263]

Wilson I, Ikonen S, Gallagher M, Eichenbaum H, Tanila H. Age-associated alterations of hippocampal place cells are subregion specific. The Journal of Neuroscience. 2005; 25(29):6877–86. [PubMed: 16033897]

Wood M, Attner M, Oliveira A, Brindle P, Abel T. A transcription factor-binding domain of the coactivator CBP is essential for long-term memory and the expression of specific target genes. Learning & Memory. 2006; 13(5):609–17. [PubMed: 16980541]

Xia Z, Guo M, Ma H. Functional analysis of novel phosphorylation sites of CREB-binding protein using mass spectrometry and mammalian two-hybrid assays. Proteomics. 2011; 11(17):3444–51. [PubMed: 21751375]

Zeng Y, Tan M, Kohyama J, Sneddon M, Watson JB, Sun YE, Xie CW. Epigenetic enhancement of BDNF signaling rescues synaptic plasticity in aging. The Journal of Neuroscience. 2011; 31(49): 17800–10. [PubMed: 22159096]

Zhang M, Poplawski M, Yen K, Cheng H, Bloss E, Zhu X, Patel H, Mobbs CV. Role of CBP and SATB-1 in aging, dietary restriction, and insulin-like signaling. PLoS Biology. 2009; 7(11):e1000245. [PubMed: 19924292]

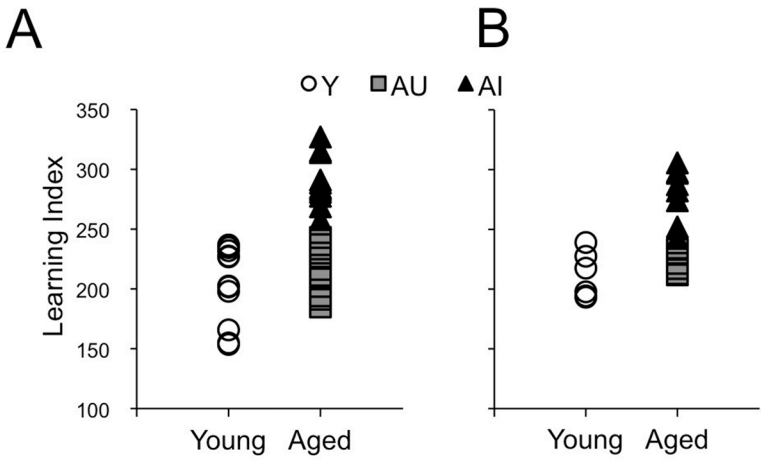

Figure 1.
Learning index scores for the individual animals. ***(A)*** Scores for the animals used in the immunohistochemical experiments. Aged animals with scores comparable to young (Y, white circles, n=11) were classified as unimpaired (AU, grey squares, n=9) and aged animals with scores outside the Y distribution were classified as impaired (AI, black triangles, n=11). ***(B)*** Scores for the animals used in the western blotting experiments (Y, n=6; AU, n=6; AI, n=8).

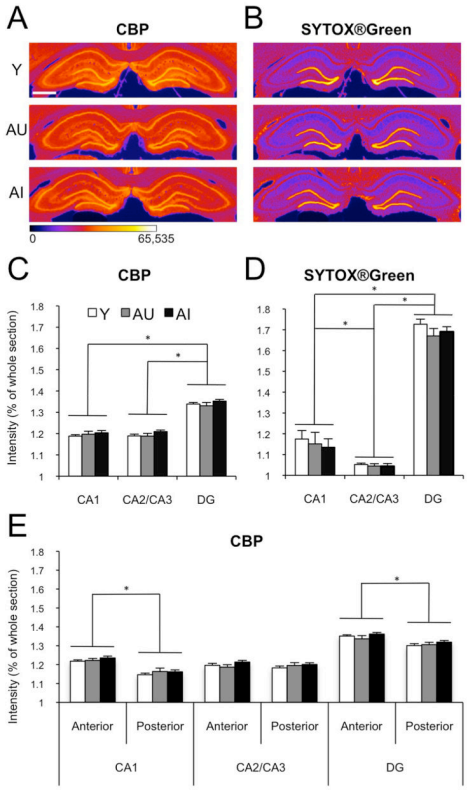

Figure 2.

CBP baseline immunofluorescence in the principal cell layers of the hippocampus, imaged on the Typhoon Trio^{+} system and quantified on ImageJ. ***(A)*** Representative CBP immunofluorescent images from one young (Y), one aged unimpaired (AU) and one aged impaired (AI) animal. The images were collected as 16-bit gray scale (0–2^{16} intensity scale) and pseudo-colored for optimal delineation of the regions of interest. Scale bar = 1mm. ***(B)*** SYTOX®Green nucleic acid counterstain of the same sections as in ***A***, processed in the same way. ***(C)*** Average intensity of CBP immunofluorescence in the principal cell layers of CA1, CA2/CA3 and DG of Y (white bars, n=11), AU (gray bars, n=9) and AI (black bars, n=11) animals, normalized to whole section CBP intensity. ***(D)*** Average intensity of the SYTOX®Green counterstain in the same animals as represented in C. ***(E)*** Average intensity of CBP immunofluorescence across the anterior-posterior axis of the hippocampus. Error bars represent standard error of the mean. *p<0.01 (repeated measures ANOVA with Bonferroni post-hoc test).

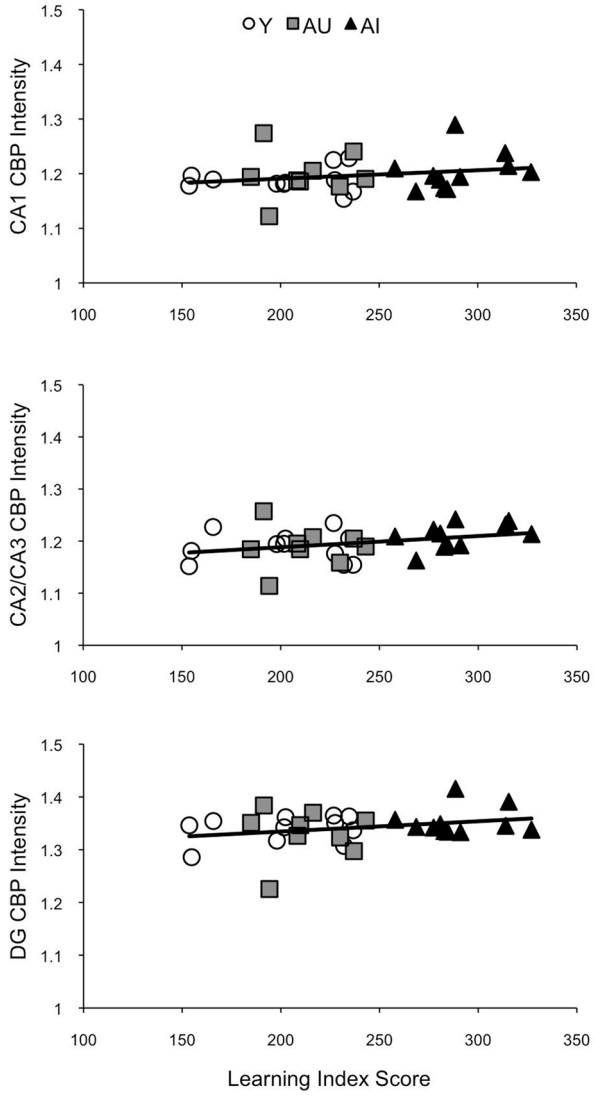

Figure 3.
Scatter plots of individual CBP immunofluorescence intensity values and the learning index scores for the principal cell fields of the hippocampus (open circles, Y animals; gray squares, AU; black triangles, AI). No significant correlations were found.

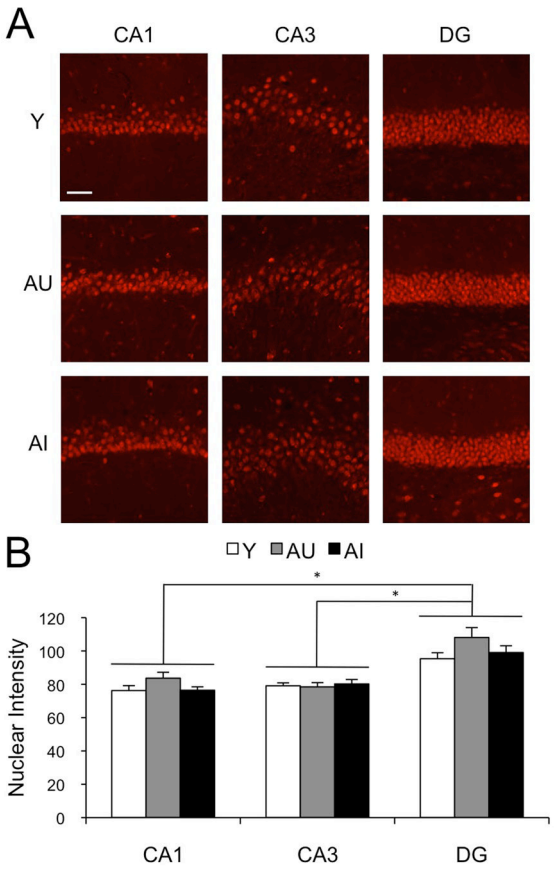

Figure 4.

Confocal CBP immunofluorescence images and quantification. ***(A)*** Representative images from the CA1, CA3 and DG of young (Y), aged unimpaired (AU) and aged impaired (AI) animals. The images were collected as 8-bit gray scale (0–2^8 intensity scale). Scale bar = 50μm. Brightness and contrast settings adjusted in the same way for all images and for presentation purposes only. ***(B)*** Average intensity of CBP immunofluorescence in the nuclei of the hippocampal subfield of Y (white bars, n=11), AU (gray bars, n=9) and AI (black bars, n=11) animals. Threshold was adjusted prior to quantification, in order to quantify nuclear labeling only. Error bars represent standard error of the mean. *$p<0.01$ (repeated measures ANOVA with Bonferroni post-hoc test).

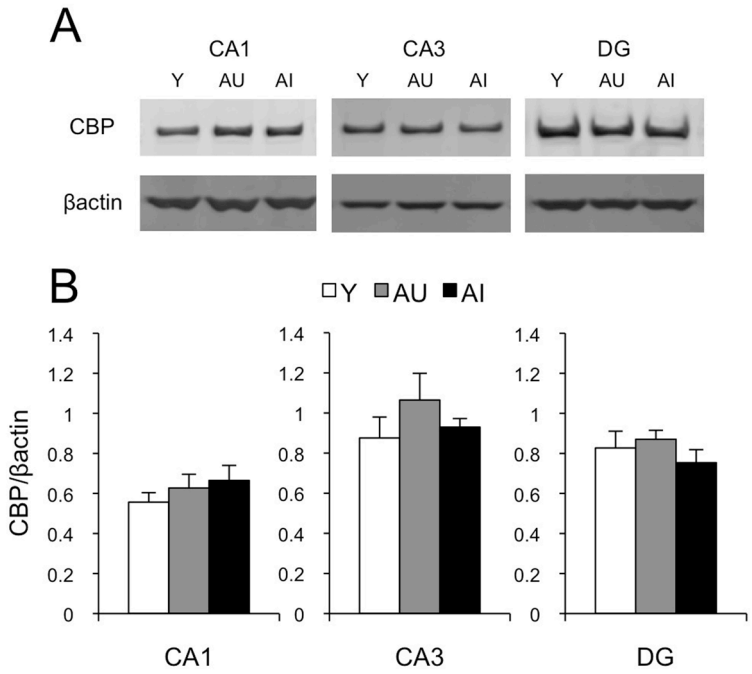

Figure 5.

Quantification of CBP levels by Western Blot. ***(A)*** Representative blots for CBP protein from micro-dissected hippocampal sub-regions CA1, CA3 and DG of young (Y), aged unimpaired (AU) and aged impaired (AI) animals. βactin was used as a loading control. ***(B)***, Average CBP protein levels, normalized to βactin in Y (n=6), AU (n=6) and AI (n=8) animals. Error bars represent the standard error of the mean. No significant differences were found.

Table 1

Pearson two-tailed r correlations between CBP immunoreactivity intensity and learning index score (*p* values are represented in *italic*).

	CA1	CA2/CA3	DG
Y	0.08 *(0.81)*	−0.02 *(0.96)*	0.29 *(0.38)*
AU	0.06 *(0.88)*	−0.01 *(0.99)*	0.02 *(0.96)*
AI	0.29 *(0.39)*	0.47 *(0.14)*	0.11 *(0.75)*
Aged (AU+AI)	0.16 *(0.50)*	0.38 *(0.10)*	0.29 *(0.22)*
All animals	0.22 *(0.23)*	0.33 *(0.07)*	0.27 *(0.14)*

Table 2

WND-CHARM accuracy at classifying images into the predefined groups: Y, AU and AI (average accuracy is 33%).

	WND-CHARM Image Classification					
	CA1		CA3		DG	
	CBP	SYTOX® Green	CBP	SYTOX® Green	CBP	SYTOX® Green
Y	32.4 ± 0.6	37.7 ± 0.6	36.7 ± 0.6	63.7 ± 0.6	47.2 ± 0.6	38.8 ± 0.6
AU	39.8 ± 0.6	36.8 ± 0.6	24.0 ± 0.5	33.5 ± 0.6	28.5 ± 0.6	49.5 ± 0.6
AI	38.6 ± 0.6	38.7 ± 0.6	50.8 ± 0.6	50.5 ± 0.6	50.9 ± 0.6	58.4 ± 0.6
Combined	**37.0 ± 0.3**	**37.7 ± 0.3**	**37.2 ± 0.3**	**49.2 ± 0.4**	**42.2 ± 0.4**	**48.9 ± 0.4**

Note: values are represented with a 95% confidence interval, calculated using the normal approximation of the binomial distribution.

Table 3

Pearson two-tailed r correlations between CBP protein levels measured by Western blot and learning index score (*p* values are represented in *italic*).

	CA1	CA3	DG
Y	−0.25 *(0.64)*	−0.02 *(0.97)*	−0.20 *(0.71)*
AU	0.17 *(0.75)*	−0.23 *(0.67)*	0.38 *(0.46)*
AI	−0.42 *(0.30)*	−0.11 *(0.80)*	−0.50 *(0.21)*
Aged (AU+AI)	−0.09 *(0.75)*	−0.31 *(0.28)*	−0.49 *(0.07)*
All animals	0.05 *(0.83)*	−0.08 *(0.75)*	−0.37 *(0.11)*